Fourier transform digital holographic adaptive optics imaging system

Changgeng Liu, Xiao Yu, and Myung K. Kim*

Digital Holography and Microscopy Laboratory, Department of Physics University of South Florida, Tampa, Florida 33620, USA

*Corresponding author: mkkim@usf.edu

Received 4 October 2012; revised 14 November 2012; accepted 15 November 2012; posted 15 November 2012 (Doc. ID 177423); published 10 December 2012

A Fourier transform digital holographic adaptive optics imaging system and its basic principles are proposed. The CCD is put at the exact Fourier transform plane of the pupil of the eye lens. The spherical curvature introduced by the optics except the eye lens itself is eliminated. The CCD is also at image plane of the target. The point-spread function of the system is directly recorded, making it easier to determine the correct guide-star hologram. Also, the light signal will be stronger at the CCD, especially for phase-aberration sensing. Numerical propagation is avoided. The sensor aperture has nothing to do with the resolution and the possibility of using low coherence or incoherent illumination is opened. The system becomes more efficient and flexible. Although it is intended for ophthalmic use, it also shows potential application in microscopy. The robustness and feasibility of this compact system are demonstrated by simulations and experiments using scattering objects.

OCIS codes: 090.1995, 010.1080, 170.4460.

1. Introduction

The concept of adaptive optics (AO) was first proposed by Babcock to address the distortion caused by the atmospheric turbulence in astronomy [1]. In 1977, Hardy *et al.* successfully demonstrated an AO system in astronomy [2]. Most of major ground-based telescopes are now equipped with AO [3,4]. Like ground-based telescopes, the human eye also suffers from many monochromatic aberrations, due to the irregularity of the cornea and eye lens, which degrade the retinal image quality. To improve the quality of the retinal images, the Shack–Hartmann sensor was first incorporated into an AO system for vision science in 1997 by Liang *et al.* [5]. Retinal images with unprecedented resolution capable of resolving individual photoreceptors were obtained using the AO system. Since then the field of AO in vision science has been rapidly growing with more and more systems being developed [6–11]. Recently, the AO system has also been applied in microscopy to reduce the aberrations induced by variations of refractive index through the sample [12]. Using the AO system, high-resolution in-depth microscopic images of some biological samples are achieved [13].

A typical AO system includes several critical hardware pieces: a spatial light modulator or deformable mirror, a lenslet array, and a second CCD camera in addition to the camera for imaging. The recently proposed digital holographic adaptive optics (DHAO) system replaces these hardware components with numerical processing for wavefront measurement and compensation of aberration through the principles of digital holography [14]. The wavefront sensing and correction by DHAO have almost the full resolution of the CCD camera. It is inherently faster than conventional AO because it does not involve feedback and iteration, and the dynamic range of deformation measurement is essentially unlimited. DHAO may offer additional novel imaging capabilities such as wider field of view (FOV) of the retina, automatic focus over the entire FOV of a curved retinal surface, topography of the retinal surface, and three-dimensional imaging of intraocular debris distribution [15–20].

1559-128X/12/358449-06$15.00/0

In the existing DHAO setup [14], the imaging sensor is put at the conjugate plane of the eye pupil. From a guide-star hologram, we can obtain the phase aberration at pupil plane. The imaging lens other than the eye lens will introduce spherical curvature that has to be removed by additional matching lens in the reference beam. And, the correct guide-star hologram is difficult to obtain. Many trials have to be performed to get a correct measurement of the phase aberration. To get a focus image, a numerical lens is added and numerical propagation is performed. If the effective CCD aperture is smaller than the pupil, the resolution will be limited. Also, it becomes impossible to employ a low coherence or incoherent light source [21–25], which may be methods of reducing the speckle noise if it becomes a real issue in the real retinal imaging. To address these limitations, the Fourier transform DHAO (FTDHAO) system is presented. The CCD is put at the exact FT plane of the eye pupil. There is no spherical curvature induced by the imaging lens, resulting in a more precise measurement of the phase aberration and a more compact system. The CCD can directly record the point-spread function (PSF) of the system, making it easier to determine the correct guide-star hologram. The CCD is also at the image plane of the target. The signal will be stronger than the existing system, especially for the phase-aberration sensing. Numerical propagation is not necessary. If the pixel is smaller than half of the diffraction-limited resolution, other parameters of the CCD have nothing to do with the resolution. So, the CCD's aperture will not affect the resolution anymore. With some modifications, low coherence or even an incoherent light source can be incorporated [21–25]. So, the system will be more flexible and applicable.

The principle of the proposed FTDHAO imaging system is different from that of the existing DHAO imaging system [14]. In the FTDHAO imaging system, the phase aberration at the eye pupil can be retrieved by the inverse FT of the guide-star hologram and the complex amplitude of full-field optical field at the eye pupil can be obtained by the inverse FT of the full-field hologram. The correction takes place at the eye pupil, instead of the CCD plane. Taking FT of the corrected field at the eye pupil, the corrected image can be obtained. Numerical propagation is not necessary. Simulations and experimental studies show the efficiency and robustness of this new DHAO system.

The paper is organized as follows: the FTDHAO apparatus is presented and the principle of this new system is described in Section 2. In Section 3, simulations are given. The experimental results are given and discussed in Section 4. Finally, the conclusions are drawn.

2. FTDHAO Apparatus and Principle

The schematic of the FTDHAO setup is illustrated in Fig. 1. The eye lens is simulated by the lens E of which the focal length f_1 equals 25 mm. R represents the retinal plane that is at the back focal plane of eye lens E. A represents the phase aberrator that is at the pupil of the eye lens. The distance between lens E and $L2$ and that between $L2$ and the CCD are equal to the focal length f_2 of $L2$, which is 200 mm in our simulations and experiments. According to [26], the optical field at the CCD plane is the two-dimensional Fourier transformation of the optical field at the eye pupil except a global prefactor. The relationship between the optical field $P(x_1,y_1)$ at the eye pupil and the field $O(x_2,y_2)$ at the CCD plane is given by [26]

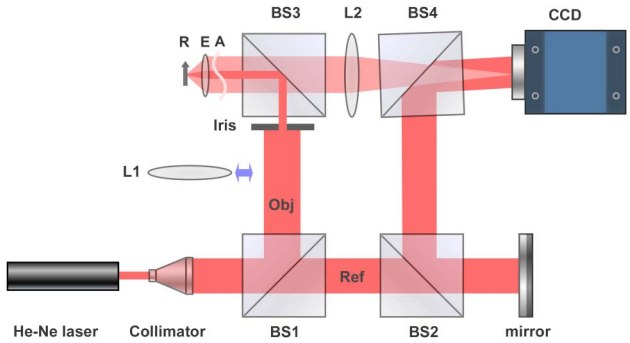

Fig. 1. (Color online) Schematic of the Fourier digital holographic adaptive optics imaging system. R, retina; E, eye lens of focal length 25 mm; A, aberrator; L1, 75 mm in focal length; L2, 200 mm; BS1–4, beamsplitters.

$$O(x_2,y_2) = \frac{1}{j\lambda f_2}\iint P(x_1,y_1) \times \exp\left[-j2\pi\frac{1}{\lambda f_2}(x_2x_1 + y_2y_1)\right]\mathrm{d}x_1\mathrm{d}y_1, \quad (1)$$

where λ is the wavelength of the light source. Ignoring the prefactor, Eq. (1) can be rewritten as

$$O(f_x,f_y) = \mathrm{FT}\{P(x_1,y_1)\}(f_x,f_y), \quad (2)$$

where

$$f_x = \frac{x_2}{\lambda f_2} \qquad f_y = \frac{y_2}{\lambda f_2}. \quad (3)$$

By holographic process, the optical field $O(f_x,f_y)$ at the CCD plane can be retrieved [16–20]. The optical field $P(x_1,y_1)$ at the eye pupil can be obtained by taking the inverse FT of it, as follows:

$$P(x_1,y_1) = \mathrm{IFT}\{O(f_x,f_y)\}(x_1,y_1). \quad (4)$$

The holographic process is realized by a modified Mach–Zehnder interferometer as shown by Fig. 1. A plane-wave reference interferes with the object field at a small angle to generate an off-axis hologram from which the object field can be reconstructed [16–20]. The small angle is realized by tilting the beamsplitter BS4 as shown in Fig. 1. For the phase-aberration measurement, a narrow collimated laser

beam of diameter about 2 mm enters the eye through the aberrator and the eye lens, which forms a focused spot on the retina—the so-called guide star. The light scatters and reflects from the guide-star spot and exits the eye with a broad coverage of the aberrator and the eye lens. A guide-star hologram is captured by the CCD. The phase aberration, $\phi(x_1, y_1)$, introduced by the aberrator and the system error can be reconstructed from the guide-star hologram. For full-field imaging, the lens $L1$ is inserted in the setup. The laser beam is focused at the front focus of the eyes lens, resulting in a collimated illumination of the retina. The exiting distorted field $P(x_1, y_2)$ at the eye pupil can be recovered by the full-field hologram. The corrected image can be described by

$$O_c(x_2, y_2) = \mathrm{FT}\{P(x_1, y_1)\exp(-j\phi(x_1, y_1))\}(f_x, f_y). \quad (5)$$

The corrected image is already focused because the CCD is also at the conjugate plane of the retina. Therefore, further numerical propagation is not necessary. To recover the optical field at the eye pupil from the digital off-axis hologram, the inverse fast Fourier transform is utilized. If the CCD has $M \times N$ square pixels with side length Δx_2, then the sampling spacings of the spatial frequency are given by

$$\Delta f_x = \frac{\Delta x_2}{\lambda f_2} \qquad \Delta f_y = \frac{\Delta y_2}{\lambda f_2}. \quad (6)$$

Then, sampling spacings at pupil plane can be given by [18–20]

$$\Delta x_1 = \frac{\lambda f_2}{M \Delta x_2} \qquad \Delta y_1 = \frac{\lambda f_2}{N \Delta x_2}. \quad (7)$$

Assume the diameter of the round eye pupil is D, and the dimension of zero order of the hologram is twice the dimension of the image or twin order. To recover the optical field at pupil plane, the pupil size D has to satisfy [27]

$$D \le \frac{\sqrt{2}\lambda f_2}{4\Delta x_2}. \quad (8)$$

For instance, if $\lambda = 0.633$ μm, $f_2 = 200$ mm, and $\Delta x_2 = 4.65$ μm as we adopt in the experiment, then the maximum D can be 9.63 mm. In most cases in ocular imaging and microscopy, the size of the pupil will not exceed 8 mm. Hence, off-axis holography is sufficient to recover the optical field in these applications.

3. Simulations

In the simulation, we use the group 4 elements 2–5 of USAF1951 resolution target to simulate the amplitude of the retina, as shown by Fig. 2(a). The FOV is 780 μm × 780 μm. A random phase noise ranging from $-\pi$ to π simulates the phase distribution of the retina, as illustrated by Fig. 2(b). All the phase profiles throughout this paper are displayed in a blue-white-red colormap that corresponds to $[-\pi\ \pi]$. The wavelength of the laser beam is set to be 0.633 μm. As a baseline, the focused image, without the aberrator in place, is given in Fig. 2(c). The CCD has 1536 × 1536 square pixels with pixel size 3.9 μm. From Eq. (6), the sampling spacing of the spatial frequency along either dimension can be calculated as 0.031 linepairs/mm. The phase aberration is simulated by the Zernike term $4\pi Z_6^2 = 4\pi(15r^6 - 20r^4 + 6r^2)\cos(2\theta)$, as shown in Fig. 2(d). The pupil size is set to be 5 mm in diameter. Figure 2(e) shows the image distorted by the phase aberration. Taking inverse FT of the distorted image field, the optical field at the pupil plane can be obtained. The phase map of this field at pupil is represented by Fig. 2(f), which is distorted by the phase aberration. The sampling spacing at the eye pupil is 21.1 μm, according to Eq. (7). In the guide-star process, we set the input beam to be 2 mm in diameter. The measured phase map is shown in Fig. 2(g). The measurement error is 0.09 wavelengths. Subtracting the measured phase aberration by Fig. 2(g) from the distorted optical field represented by Fig. 2(f), the corrected optical field at pupil can be obtained, as shown by Fig. 2(h). Taking FT of this corrected optical field, the corrected image is achieved, as shown in Fig. 2(i). The corrected image shows remarkable improvement in resolution. Other simulation samples for various types and strengths of phase aberrations show the FTDHAO is quite robust, especially for fairly severe aberrations.

4. Experimental Results and Discussion

An He–Ne laser is used as the light source in our experiments. The wavelength is 0.633 μm. The first sample under test is a positive USAF 1951 resolution target with a piece of Teflon tape tightly attached behind. The specular reflection is blocked by the pupil whose size is set to be 5 mm in diameter. A piece of clear broken glass serves as the phase aberrator. A set of image data is shown in Fig. 3. The FOV on the retinal plane is 573 μm × 430 μm with 1024 × 768 pixels. The hologram with full-field illumination, without the aberrator in place, is shown in Fig. 3(a). The angular spectrum, i.e., the inverse FT of the hologram, is shown in Fig. 3(b), with the highlighted elliptical area on the upper right representing the image-order term for extracting the complex optical field at the pupil plane [19,20]. The filtered angular spectrum of Fig. 3(b) is the complex optical field at the pupil plane. The phase map of this field is shown in Fig. 3(c). The sampling spacings along horizontal and vertical directions are 26.6 and 35.4 μm, respectively. The number of pixels occupied by the elliptical area is 190 × 140, which corresponds to a circle of diameter 5 mm, the same as the actual pupil size. The reconstructed image that serve as a baseline is shown in Fig. 3(d). Figure 3(e) shows the full-field hologram with the aberrator in place. The angular spectrum is shown in Fig. 3(f). The phase map of the

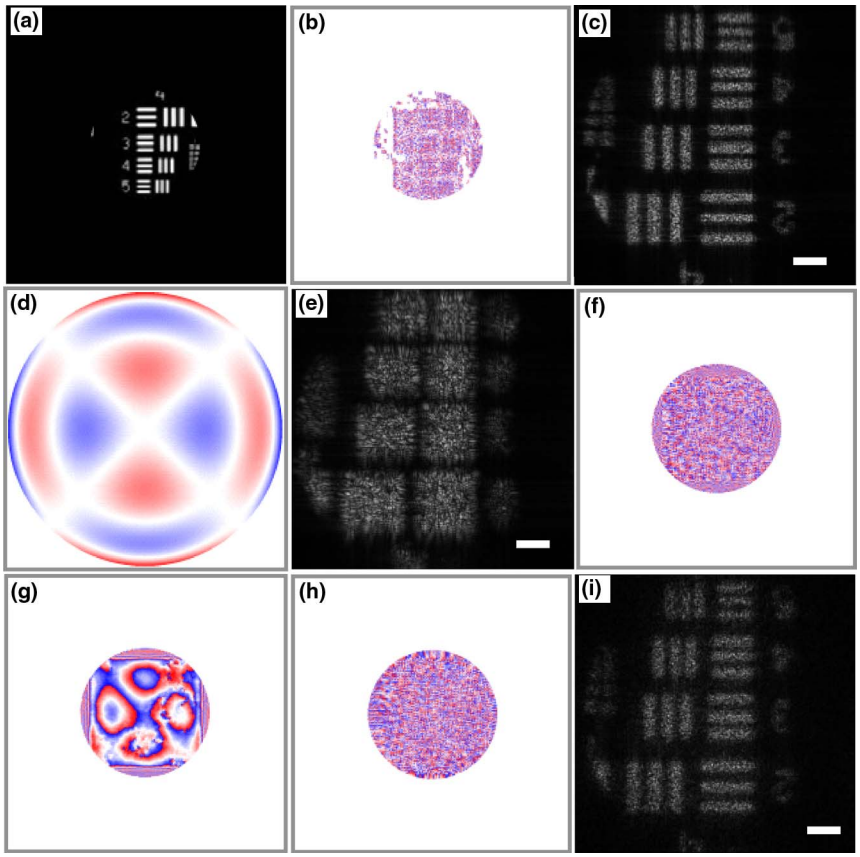

Fig. 2. (Color online) Simulations. (a), (b) Simulated amplitude and phase. The phase map is represented by a blue-white-red colormap that corresponds to $[-\pi, \pi]$. (c) Image without aberrator in place. (d) Simulated phase aberration. (e) Distorted image. (f) Phase map of distorted field at the eye pupil. (g) Measured phase aberration at the eye pupil. (h) Phase map of the corrected field at pupil. (i) Corrected image. Scale bar: 100 μm.

distorted optical field at pupil is shown in Fig. 3(g). Figure 3(h) shows the distorted image where the resolution is totally lost due to the phase aberration. The guide-star hologram is shown in Fig. 3(i). The dashed circle represents a spatial spectral filter with 3.7 linepairs/mm in diameter. The angular spectrum

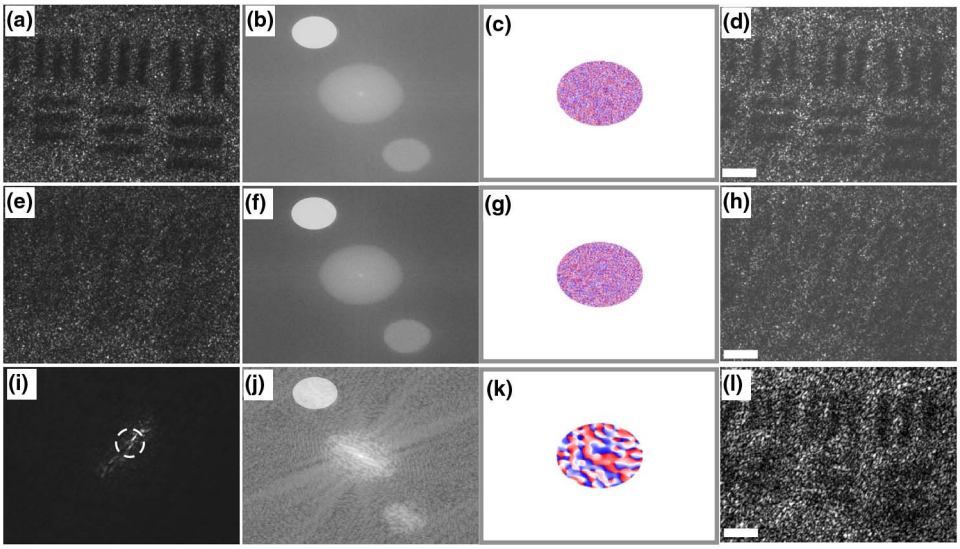

Fig. 3. (Color online) Experimental results on USAF 1951 resolution target. (a) Undistorted full-field hologram. (b) Angular spectrum of (a), displayed in logarithmic scale. (c) Phase map of part of (a) filtered by the highlighted elliptical area. (d) Reconstructed baseline image. (e) Distorted full-field hologram. (f) Angular spectrum of (e). (g) Distorted phase map. (f) Distorted image. (i) Guide-star hologram. (j) Angular spectrum of part of (i) represented by the dashed circle. (k) Measured phase aberrations. (l) Corrected image. Scale bar: 100 μm.

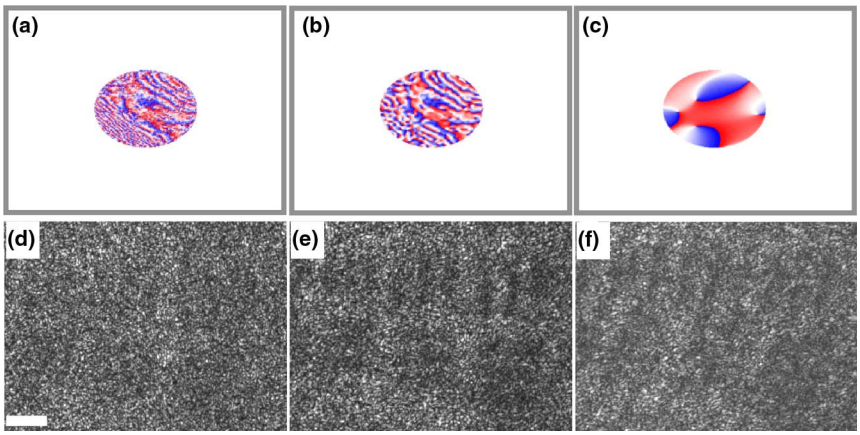

Fig. 4. (Color online) Corrected images with varying spatial spectral filters. (a)–(c) Measured phase aberrations with filter diameters 28.4, 7.4, and 0.74 linepairs/mm, respectively. (d)–(f) Corrected images by the phase measurements in upper panel. Scale bar: 100 μm.

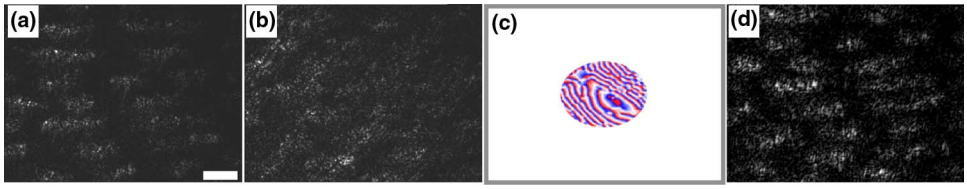

Fig. 5. (Color online) FTDHAO on onion tissue. (a) Baseline image, (b) distorted image, (c) measured aberration, and (d) corrected image. Scale bar: 100 μm.

of filtered hologram is shown in Fig. 3(j). The measured phase aberration is given by Fig. 3(k). The RMS of phase distortion is 0.49 μm, a rather severe value compared to those expected in the normal population [7].

Subtracting Figs. 3(k) from 3(g) and taking FT, the corrected image is obtained, as illustrated by Fig. 3(l), which shows significant improvement in resolution and image quality compared with the distorted image given Fig. 3(h). The resolution is completely recovered by the FTDHAO correction. A proper spatial spectral filter plays important role in phase-aberration measurement. Because the phase aberration has a certain bandwidth, most information lies in a limited spatial-frequency range. Outside this range, the information bears negligible effect on compensating for the distorted image. Therefore, a proper filter can recover most phase aberration while effectively reducing the noise for scattering samples. To illustrate this argument, a comparison of corrected images is given in Figs. 4(a)–4(c) are the phase aberration measurements when filter sizes are 28.4, 7.4, and 0.74 linepairs/mm. The corresponding images are shown in the lower panel from Figs. 4(d) to 4(f). When the filter is too large, although almost all the phase aberration can be recovered, the noise is too strong and the corrected image is messed up by the noise, as shown by Fig. 4(d). When filter size decreases to 7.4 linepairs/mm, the resolution is recovered while noise still degrades the corrected image quality, as shown in Fig. 4(e). When the filter size is too small, the phase aberration is lost. Therefore, there is no improvement in the corrected image as shown by Fig. 4(f). The optimal filter size depends on the aberration and degree of surface roughness of the target. The filter size will tend to decrease as the degree of surface roughness increases. For this specific sample, the optimal filter size is about 3.7 linepairs/mm.

A second example to be tested is the onion tissue. The experimental results are shown in Fig. 5. The focused image without aberrator serves as a baseline, as shown in Fig. 5(a). The distorted image is shown in Fig. 5(b). A spatial spectral filter of a diameter 7.4 linepairs/mm is applied to the guide-star hologram. The measured phase aberration from this filtered hologram is given by Fig. 5(c). The corrected image is shown in Fig. 5(d) and shows significant improvement in resolution and quality compared to the distorted image by Fig. 5(b).

5. Conclusions

A novel DHAO imaging system is proposed. The CCD is located at FT plane of the pupil of the eye lens. The PSF can be directly visualized, making it practically easy to determine the correct guide-star hologram. In FTDHAO, numerical propagation is avoided. The limit of the CCD aperture on the resolution is eliminated and the low coherence or even incoherent illumination becomes possible [21–23]. Although FTDHAO is designed for ophthalmic use, it also shows potential applications in in-depth biomedical microscopy [12,13]. The basic principles and feasibility of the FTDHAO imaging system are demonstrated by simulations and experimental results. FTDHAO is proved to be more compact, flexible,

and efficient compared to the system proposed in [14].

The research reported in this paper was supported by the National Eye Institute of the National Institute of Health under Award No. R21EY021876. The content is solely the responsibility of the authors and does not necessarily represent the official views of the National Institute of Health.

References

1. H. W. Babcock, "The possibility of compensating astronomical seeing," Publ. Astron. Soc. Pac. **65**, 229–236 (1953).
2. J. W. Hardy, J. E. Lefebvre, and C. L. Koliopoulos, "Real-time atmospheric compensation," J. Opt. Soc. Am. **67**, 360–369 (1977).
3. M. A. van Dam, D. Le Mignant, and B. A. Macintosh, "Performance of the Keck observatory adaptive optics system," Appl. Opt. **43**, 5458–5467 (2004).
4. M. Hart, "Recent advances in astronomical adaptive optics," Appl. Opt. **49**, D17–D29 (2010).
5. J. Liang, D. R. Williams, and D. Miller, "Supernormal vision and high-resolution retinal imaging through adaptive optics," J. Opt. Soc. Am. A **14**, 2884–2892 (1997).
6. A. Roorda, F. Romero-Borja, W. J. Donnelly III, H. Queener, T. J. Herbert, and M. C. W. Campbell, "Adaptive optics scanning laser ophthalmoscopy," Opt. Express **10**, 405–412 (2002).
7. K. M. Hampson, "Adaptive optics and vision," J. Mod. Opt. **55**, 3425–3467 (2008).
8. I. Iglesias, R. Ragazzoni, Y. Julien, and P. Artal, "Extended source pyramid wave-front sensor for the human eye," Opt. Express **10**, 419–428 (2002).
9. N. Doble, G. Yoon, L. Chen, P. Bierden, B. Singer, S. Olivier, and D. R. Williams, "Use of a microelectromechanical mirror for adaptive optics in the human eye," Opt. Lett. **27**, 1537–1539 (2002).
10. S. R. Chamot, C. Dainty, and S. Esposito, "Adaptive optics for ophthalmic applications using a pyramid wavefront sensor," Opt. Express **14**, 518–526 (2006).
11. Q. Mu, Z. Cao, D. Li, and L. Xuan, "Liquid crystal based adaptive optics system to compensate both low and high order aberrations in a model eye," Opt. Express **15**, 1946–1953 (2007).
12. M. J. Booth, "Adaptive optics in microscopy," Philos. Trans. R. Soc. A **365**, 2829–2843 (2007).
13. M. J. Booth, D. Debarre, and A. Jesacher, "Adaptive optics for biomedical microscopy," Opt. Photon. News **23**(1), 22–29 (2012).
14. C. Liu and M. K. Kim, "Digital holographic adaptive optics for ocular imaging: proof of principle," Opt. Lett. **36**, 2710–2712 (2011).
15. U. Schnars and W. Jüptner, "Direct recording of holograms by a CCD target and numerical reconstruction," Appl. Opt. **33**, 179–181 (1994).
16. E. Cuche, P. Marquet, and C. Depeursinge, "Digital holography for quantitative phase-contrast imaging," Opt. Lett. **24**, 291–293 (1999).
17. C. Mann, L. Yu, C. Lo, and M. K. Kim, "High-resolution quantitative phase-contrast microscopy by digital holography," Opt. Express **13**, 8693–8698 (2005).
18. C. Liu, D. Wang, and Y. Zhang, "Comparison and verification of numerical reconstruction methods in digital holography," Opt. Eng. **48**, 1058021 (2009).
19. M. K. Kim, "Principles and techniques of digital holographic microscopy," SPIE Rev. **1**, 018005 (2010).
20. M. K. Kim, *Digital Holographic Microscopy: Principles, Techniques, and Applications*, Springer Series in Optical Sciences (Springer Science+Business Media, 2011), pp. 55–93.
21. F. Dubois, L. Joannes, and J. C. Legros, "Improved three-dimensional imaging with digital holography microscope with a source of partial spatial coherence," Appl. Opt. **38**, 7085–7094 (1999).
22. G. Pedrini and H. J. Tiziani, "Short-coherence digital microscopy by use of lensless holographic imaging system," Appl. Opt. **41**, 4489–4496 (2002).
23. M. K. Kim, "Adaptive optics by incoherent digital holography," Opt. Lett. **37**, 2694–2696 (2012).
24. F. Dubois and C. Yourassowsky, "Full off-axis red-green-blue digital holographic microscope with LED illumination," Opt. Lett. **37**, 2190–2192 (2012).
25. R. Kelner and J. Rosen, "Spatially incoherent single channel digital Fourier holography," Opt. Lett. **37**, 3723–3725 (2012).
26. J. Goodman, *Introduction to Fourier Optics*, 3rd ed. (Roberts & Company, 2005).
27. N. Pavillon, C. S. Seelamantula, J. Kühn, M. Unser, and C. Depeursinge, "Suppression of the zero-order term in off-axis digital holography through nonlinear filtering," Appl. Opt. **48**, H186–H195 (2009).